Wide-Speed Direct Torque and Flux Control for Interior PM Synchronous Motors Operating at Voltage and Current Limits

Chan-Hee Choi, *Student Member, IEEE*, Jul-Ki Seok, *Senior Member, IEEE*, and Robert D. Lorenz, *Fellow, IEEE*

***Abstract*—This paper proposes a wide-speed direct torque and flux control method associated with the inverter voltage and current constraints of interior permanent-magnet synchronous motors. The proposed approach has potential advantages controlling torque and flux linkage at the voltage and current limits, since no integrators are employed for torque control or flux weakening. The transition between the non-limited operation and maximum voltage modulation can be achieved automatically without modifying the control law. To confirm this, we provide a graphical and analytical analysis that naturally leads to a unique stator voltage vector selection on the hexagon. The proposed controller can maximize the available inverter voltage and generate a higher output torque than conventional current vector controllers at high speeds. The method developed in this paper also retains the beneficial features of classical direct torque control, such as its fast dynamics and direct manipulation of the stator flux linkage for flux weakening.**

***Index Terms*—Available inverter voltage maximization, interior permanent-magnet synchronous motors (IPMSMs), inverter voltage and current constraints, wide-speed direct torque and flux control (WS-DTFC).**

I. Introduction

INTERIOR permanent-magnet synchronous motors (IPMSMs) have received a great deal of attention in the field of high-performance drive applications due to their unique features, such as their high efficiency, high power density, and wide constant power speed range [1]. One important issue that is relevant to the control of IPMSMs is the extension of the dc link voltage utilization, since the efficiency and power density of motors and drive systems, such as those used in automotive applications, are crucial due to the limited battery power. A number of methods of exploiting the available bus voltage have been reported over a wide range of speeds based on current vector control (CVC) [2]–[4]. However, since current control leaves the motor flux linkage in the open loop state, the dynamic ability to vary the flux linkage is generally more limited. Moreover, open loop air-gap torque dynamics are also limited by the current controller dynamics, and accurate current regulation is problematic when operating near the voltage limit of the inverter. A modified CVC methodology was proposed [5] in order to extend the linear voltage limit of CVC to quasi six-step ranges. This is achieved by introducing extra control functions and a tuning gain, which should be carefully selected based on a complex tradeoff between voltage utilization and current control dynamics. The add-on algorithm needs to be integrated with the controller that prevents the streamlined batch-analysis and design over a wide range of speeds resulting from the multiple control laws.

Recently, some modified direct torque and flux control (DTFC) schemes have been reported for high-performance ac motor drives [6]–[9]. Despite their improved control performance over that of classical direct torque control algorithms, there exist some limitations associated with their voltage limit operations. In [6], [7], a variable control structure with switching logic tables was implemented to enable the adjustment of the flux command. The drawback of using such methods is the added complexity of implementing a different control law when operating at high speeds. The system in [8], [9] controls the stator flux magnitude and torque output by using a PI regulator with a fixed PWM switching frequency. Unfortunately, the integrators in the regulator would wind up and cause the system to exhibit poor dynamic performance at the operating limits. With these methods, the realization of maximum voltage utilization fails, because they consider the voltage limit as a circle instead of a hexagon. Consequently, this control methodology based on the linear voltage limit increases the copper loss and requires multiple control laws for the transition between flux weakening and maximum voltage utilization. These adverse consequences arise due to the adherence of the system to the control structure employing the PI regulator at the operating limits [5]. In the aforementioned studies on DTFC based on the space vector modulation, one of the main reasons for employing the PI regulator is the fact that the nonlinear cross-coupling of the voltage manipulated input, yielding both the air-gap torque and stator flux linkage, is not directly solvable and cannot be directly decoupled in continuous time. Because the decoupling of the

Manuscript received January 4, 2012; revised May 1, 2012; accepted May 15, 2012. Date of publication November 29, 2012; date of current version January 16, 2013. Paper 2011-IDC-801.R1, presented at the 2011 IEEE Energy Conversion Congress and Exposition, Phoenix, AZ, September17–22, and approved for publication in the IEEE Transactions on Industry Applications by the Industrial Drives Committee of the IEEE Industry Applications Society. This work was supported by a National Research Foundation of Korea Grant funded by the Korean government(MEST) (2011-0000893).

C.-H. Choi and J.-K. Seok are with the School of Electrical Engineering, Yeungnam University, Kyungsan 712-749, Korea (e-mail: johnny@ynu.ac.kr; doljk@ynu.ac.kr).

R. D. Lorenz is with the Wisconsin Electric Machines and Power Electronics Consortium, University of Wisconsin, Madison, WI 53706 USA (e-mail: r.d.lorenz@ieee.org).

Color versions of one or more of the figures in this paper are available online at http://ieeexplore.ieee.org.

Digital Object Identifier 10.1109/TIA.2012.2229684

cross-coupling is not straightforward in the continuous time motor model, a different control solution is necessary.

There have been many attempts to use deadbeat-DTFC (DB-DTFC) as a high-performance control law for ac motors [10]–[12]. DB-DTFC utilizes an inverse discrete time motor model to determine the stator voltage vector that would achieve the desired torque and stator flux magnitude at the end of the next PWM interval. Here, a suitable DTFC solution correctly decouples the nonlinear cross-coupling of the applied voltage and provides the energy input required for both states to be achieved in discrete time without adopting a PI regulator. However, in these works, insufficient information is available to determine the stator voltage vector during a wide range of operation at elevated speeds.

In this paper, we propose a wide-speed DTFC (WS-DTFC) method associated with the inverter voltage and current constraints of IPMSMs. In the proposed approach with a constant switching frequency, the drive system can provide fast and non-oscillatory dynamics under voltage limits, since no integrators are employed for torque and flux linkage control in the flux weakening region. The automatic transition to the flux weakening mode is achieved with a single voltage selection rule. This implies that a single control law is required to generate the output voltage command in the entire operating region, unlike in the existing control methods. To support this hypothesis, we provide a graphical and analytical analysis that naturally leads to a unique stator voltage trajectory for WS-DTFC. The method developed in this paper maintains the beneficial features of classical direct torque control. Sets of a comprehensive collection of experiments are used to evaluate and verify the feasibility of the presented idea.

II. Principle of DB-DTFC Under Non-Limited Condition

The output torque of the IPMSM based on the flux linkage is simply given by

$$T_e = \frac{3}{4}P\left(\lambda^r_{ds} i^r_{qs} - \lambda^r_{qs} i^r_{ds}\right) \tag{1}$$

where λ^r_{dqs} and i^r_{dqs} represent the d–q axis stator flux linkage and the current vector in the rotor reference frame, respectively, and P denotes the number of poles.

In order to form the DB-DTFC law, the following torque differential equation can be written as

$$\dot{T}_e = \frac{3}{4}P\left(\dot{\lambda}^r_{ds} i^r_{qs} + \lambda^r_{ds}\dot{i}^r_{qs} - \dot{\lambda}^r_{qs} i^r_{ds} - \lambda^r_{qs}\dot{i}^r_{ds}\right). \tag{2}$$

The rate of change of the torque can be modeled over a PWM period T_s as a discrete time system with latched voltage input. This forms the basis for the DB-DTFC regulator [12] as

$$v^r_{qs}(k)T_s = M\, v^r_{ds}(k)T_s + B \tag{3}$$

where

$$M = \left(\frac{(L_q - L_d)\lambda^r_{qs}(k)}{(L_q - L_d)\lambda^r_{ds}(k) - L_q\lambda_{\rm pm}}\right)$$

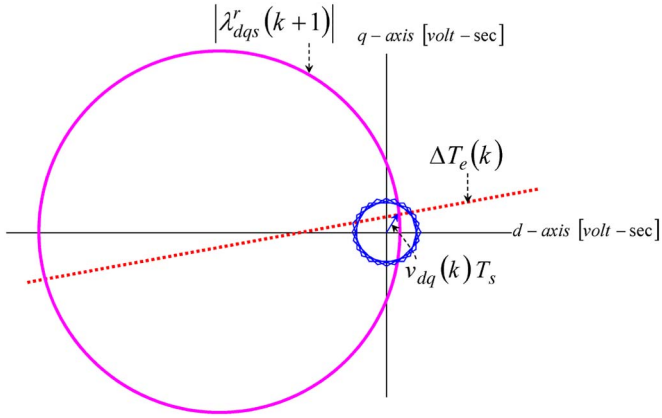

Fig. 1. Graphical solution in the non-limited region ($\omega_r = 0.33\omega_b$).

$$B = -\left(\frac{L_d L_q}{(L_q - L_d)\lambda^r_{ds}(k) - L_q\lambda_{\rm pm}}\right) \cdot \begin{bmatrix} \frac{4}{3P}\Delta T_e(k) - \frac{R_s T_s \lambda^r_{qs}(k)}{L_d^2 L_q^2}\left\{\left(L_q^2 - L_d^2\right)\lambda^r_{ds}(k) - L_q^2\lambda_{\rm pm}\right\} \\ -\frac{\omega_r T_s}{L_d L_q}\left\{(L_q - L_d)\left(\lambda^{r2}_{ds}(k) + \lambda^{r2}_{qs}(k)\right) - L_q\lambda^r_{ds}(k)\lambda_{\rm pm}\right\} \end{bmatrix}$$

and $\Delta T_e(k) = T_e(k+1) - T_e(k)$. v^r_{dqs} is the d–q axis stator voltage vector, L_{dq} indicates the d–q axis inductance, $\lambda_{\rm pm}$ is the flux linkage of the PM, R_s represents the stator resistance, and ω_r is the rotor angular velocity.

For the operating conditions when the voltage is not near the limit, the stator flux linkage would be

$$\begin{aligned} \lambda^{*2}_s &= \lambda^r_{ds}(k+1)^2 + \lambda^r_{qs}(k+1)^2 \\ &= \left\{v^r_{ds}(k)T_s + \left(\lambda^r_{ds}(k) + \omega_r\lambda^r_{qs}(k)T_s\right)\right\}^2 \\ &\quad + \left\{v^r_{qs}(k)T_s + \left(\lambda^r_{qs}(k) - \omega_r\lambda^r_{ds}(k)T_s\right)\right\}^2. \end{aligned} \tag{4}$$

Combining (3) and (4) provides a unique stator V–s solution that produces both the desired change in the output torque and stator flux magnitude at each discrete time step. Fig. 1 shows a graphical representation of the stator voltage solutions in the d–q V–s plane at 33% of the based speed. The desired change in the torque of (3) forms a dotted line in the complex stator V–s plane and is shown in red. The stator flux linkage of (4) forms a large circle which is shown in pink. Among the multiple possible stator voltage vectors, two of them fall on the constant stator flux linkage circle. Here, the voltage limit appears in the form of a small rotating hexagon over the T_s sample time interval. The voltage vector which falls inside of the voltage limits is chosen as a feasible solution because it is the only achievable voltage in the next sampling time.

Fig. 2 shows a zoomed view around the feasible voltage vector of Fig. 1 at a certain operating instant. The solution of (3) and (4) lies within the current (ellipse in black) and voltage (hexagon in blue) limits under the non-limited condition. Here, the stator flux command can be modified by a given Maximum Torque Per Ampere (MTPA) strategy. Increasing the motor speed forces the operating point to approach the voltage limit boundary, as shown in Fig. 3. This speed is called the base speed (ω_b), where the flux weakening operation starts.

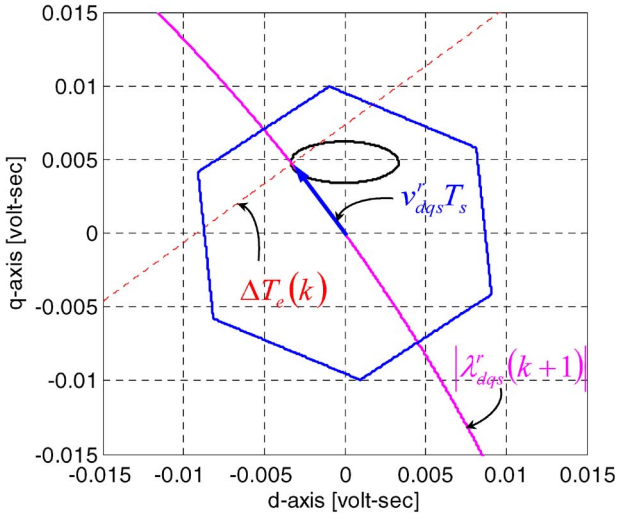

Fig. 2. Feasible solution in the non-limited region ($\omega_r = 0.33\omega_b$).

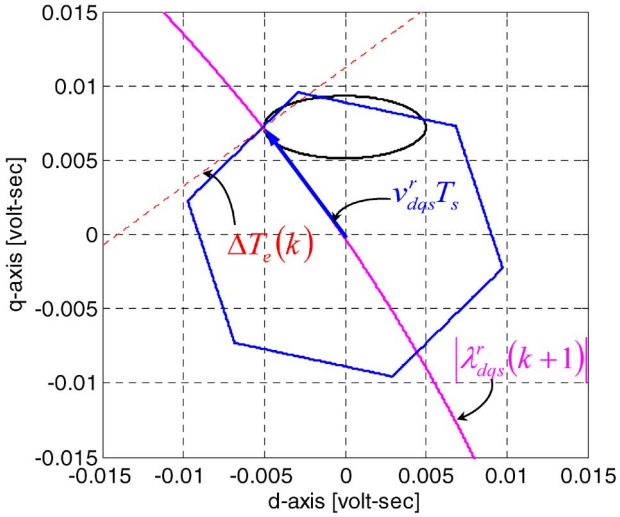

Fig. 3. Feasible solution at base speed ($\omega_r = \omega_b$).

III. Wide-Speed DTFC at Operating Limits

In this paper, the hexagon-shaped boundary is considered as a voltage limit for achieving the efficiency enhancement or the maximum voltage utilization over a wide operating region. This can be a very attractive control method for automotive applications to achieve better fuel economy and extend the operating range.

Above the base speed as shown in Fig. 4(a), the deadbeat command voltage vector, which is at the intersection of (3) and (4), lies outside of the voltage limit. In this operation, the command voltage vector should be scaled back to the physical limits. Here, three different vectors can be possible solutions as shown in Fig. 4(a). Point "a" is on the voltage limit and can achieve the maximum torque increase, but it does not satisfy the current limit condition. Point "b" satisfies both physical constraints, but it does not utilize the full current capacity. Point "c" (labeled $v^{r'}_{dqs}(k)T_s$) is the best option to develop the largest torque, while the flux decreases at a given rotor speed.

As shown in Fig. 4(b), this modification causes the stator flux circle to move toward the new voltage vector in the next step.

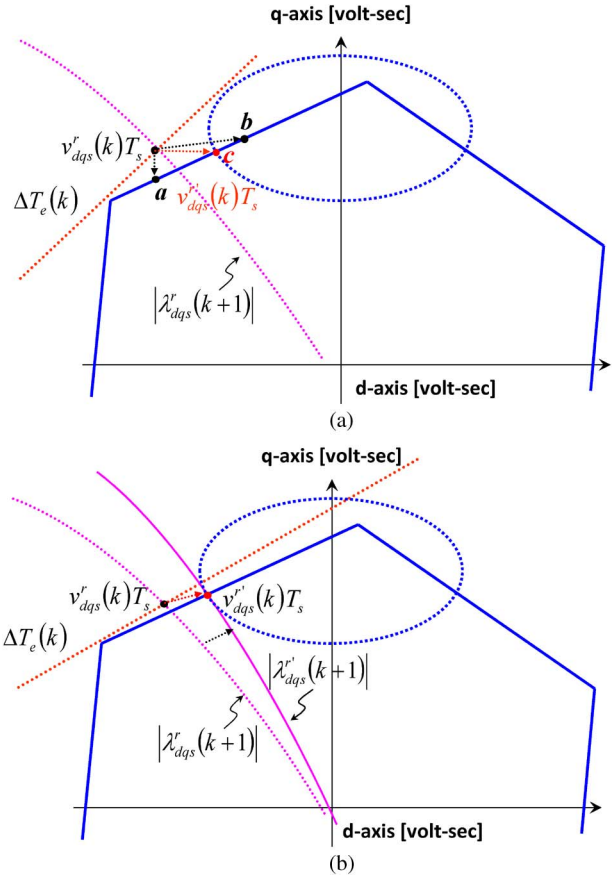

Fig. 4. Proposed flux weakening strategy ($\omega_r > \omega_b$). (a) Command voltage options outside voltage limit. (b) Command voltage modification.

Then, the stator current at the next sample time will exist on the current limit as

$$i^r_{ds}(k+1)^2 + i^r_{qs}(k+1)^2 = I^2_{s\max} \tag{5}$$

where $I_{s\max}$ represents the maximum current limited by the inverter current rating.

For the full utilization of the physical resource, both the voltage and current constraints should be considered, while maintaining the DB-DTFC features, to modify the command voltage vector at point "c." The modified voltage will be on the hexagon-shaped voltage limit. Fig. 5(a) shows a typical snapshot of the voltage limit for a given dc link voltage $V_{\rm dc}$ when the rotating angle is zero ($\theta_r = 0$). It has six equilateral triangles in the synchronous d–q V–s plane. Here, each triangle is referred to as a sector numbered as $\sec_n (n = 1, 2, \ldots, 6)$. An adjacent sector shares the vertex defined as $\boldsymbol{p}_n = (p_{nd}, p_{nq})$.

The voltage limit hexagon rotates in the reverse direction with respect to the rotor angle, as shown in Fig. 5(b). This rotation results in the variation of the d–q vertex components. For the calculation of $\boldsymbol{p}_n$, it is useful to consider the following transformation of the vertex:

$$\boldsymbol{p}_n = R^{-1}(\theta_r)\begin{bmatrix} p_{nd0} \\ p_{nq0} \end{bmatrix} \tag{6}$$

where p_{nd0} and p_{nq0} are the tip values at $\theta_r = 0$. The identification of the sector adjacent to the current limit is the first step

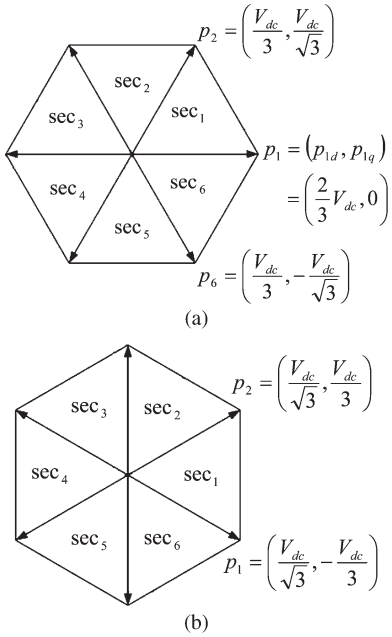

Fig. 5. Space vector diagram in the synchronous d–q V–s plane. (a) Voltage limit hexagon at $\theta_r = 0$. (b) Voltage limit hexagon at $\theta_r = +\pi/6$.

in the selection of the modified stator voltage command. Then, the boundary of each sector can be obtained as

$$v_{qs}^{r}(k)T_s = M_n\, v_{ds}^{r}(k)T_s + B_n \tag{7}$$

where

$$M_n = \frac{p_{(n+1)q} - p_{nq}}{p_{(n+1)d} - p_{nd}}$$
$$B_n = -M_n p_{nd} + p_{nq}.$$

The modified stator flux linkage can be rewritten as a function of the stator currents as follows:

$$\lambda_{ds}^{r'}(k+1) = L_d i_{ds}^{r}(k+1) + \lambda_{\mathrm{pm}}$$
$$\lambda_{qs}^{r'}(k+1) = L_q i_{qs}^{r}(k+1). \tag{8}$$

Substituting (8) into (5), the current limit is given by

$$\left(\frac{\lambda_{ds}^{r}(k+1) - \lambda_{\mathrm{pm}}}{L_d}\right)^2 + \left(\frac{\lambda_{qs}^{r'}(k+1)}{L_q}\right)^2 = I_{s\max}^2. \tag{9}$$

Combining (7) and (9), a new stator flux linkage command ($\lambda_s^{*\prime} = \lambda_{dqs}^{r'}(k+1)$) can be obtained. Then, a unique modified stator V–s solution $v_{dqs}^{r'}(k)T_s$ is also obtained as (10) to maximize the output torque under this physical constraint

$$v_{qs}^{r'}(k) = -\beta - \mathrm{sgn}(\omega_r)\cdot\sqrt{\frac{\beta^2 - 4\alpha\gamma}{2\alpha}}$$
$$v_{ds}^{r'}(k) = \frac{v_{qs}^{r'}(k) - B_n}{M_n} \tag{10}$$

where $\alpha = L_q^2 M_n^2 + L_d^2$, $\beta = -(2\omega_r \lambda_{\mathrm{pm}} L_q^2 M_n^2 + 2B_n L_d^2)$, and $\gamma = (\omega_r \lambda_{\mathrm{pm}} L_q M_n)^2 + (L_d B_n)^2 - (I_{s\max}\lambda_{\mathrm{pm}} L_d L_q M_n)^2$.

Here, it is not possible to achieve a deadbeat torque response for the desired value, but it is possible to achieve part of the desired change in torque. With this algorithm, although a deadbeat torque response can be partly achieved, the maximum voltage and current utilization are always guaranteed in the flux weakening region. The basic principle of the wide-speed DTFC is to ensure the direct control of the actual flux over the whole range of speeds and also a smooth transition between the constant flux region and the flux weakening region, without requiring any information on the base speed. The selected voltage trajectory automatically moves toward the intersection of the current and voltage limit with the speed elevation, as shown in Fig. 4(b). The proposed scheme self-regulates the stator flux without requiring any extra tuning parameters to be adjusted, allowing for satisfactory operation over the whole range of speeds. This is advantageous as only one control law needs to be developed.

In the proposed wide-speed DTFC method, the intersection of the current limited ellipse and the rotating hexagon becomes the command voltage vector at the next sampling instant. Note that the current limited ellipse moves along the positive q-axis direction with increasing speed, while one of the sides of each equilateral triangle crosses the current limit locus. Thus, the trajectories of the selected intersection are not fixed, but fluctuate on the current limited curve.

Fig. 6 shows a comparison of the selected command voltage waveforms with different rotor speeds. At the base speed in Fig. 6(a), the fluctuated interval, $\Delta v_{dqs}^{r}(k)T_s$, of the d–q voltage components is quite balanced because the selected voltages in the d–q plane stay between inscribed and circumscribed circle. Thus, additional distortion is rarely found in the output phase voltage waveform in the abc reference frame. In contrast, at the maximum speed in Fig. 6(b) where the current limit ultimately reaches the inscribed circle, a group of d–q voltage components are laid on the region corresponding to the unbalanced d–q V–s interval. Hence, as shown in Fig. 7, the phase voltage waveform in the abc reference frame progressively includes a certain amount of harmonics with multiples of six times the fundamental frequency in the synchronous coordinate with increasing rotor speed. Note that the add-on harmonics present are the $6n \pm 1$ (n is a non-zero integer) components in the abc reference frame. For applications, where the add-on harmonics are critical, limiting the d-axis fluctuating interval, $\Delta v_{ds}^{r}(k)T_s$, can improve the situation by sacrificing the corresponding voltage or current utilization.

Note that the successful command voltage selection of (10) in the flux weakening mode can be achieved as long as there is no drift of the motor parameter, as shown in Fig. 8. In practice, however, this is not always the case, and, therefore, the motor parameters of the current limit should be estimated and updated [13].

Fig. 9(a) shows an overall block diagram of the control system augmented to include the proposed DTFC algorithm. For the stator flux linkage estimation, a discrete time Gopinath-style stator flux linkage observer for IPMSMs is employed [12]. The stator current in the next sample time instant is also estimated using the discrete time version of the stator current observer to enhance the control performance. Fig. 9(b) shows the operational flow of the proposed DTFC, where the deadbeat control is carried out under non-limited condition

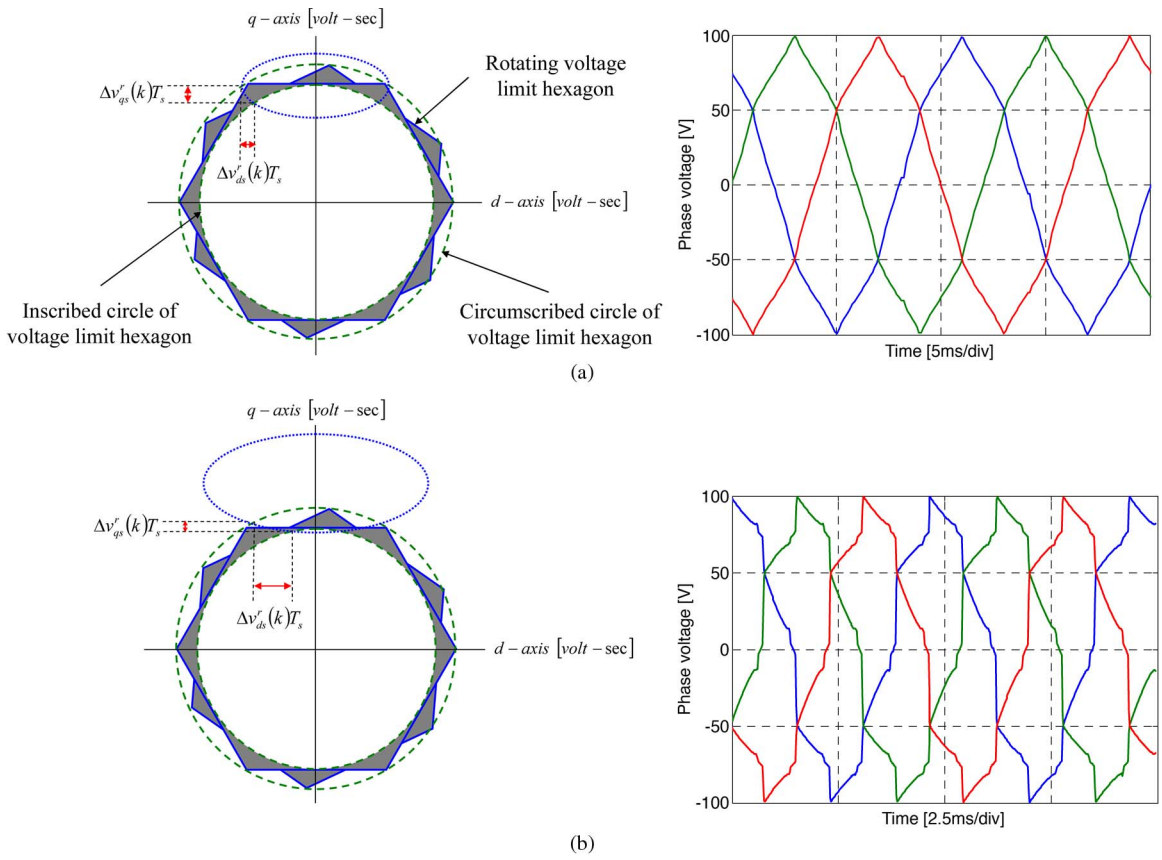

Fig. 6. Output voltage waveforms with the rotor speed. (a) Selected voltage at the base speed. (b) Selected voltage at the maximum speed.

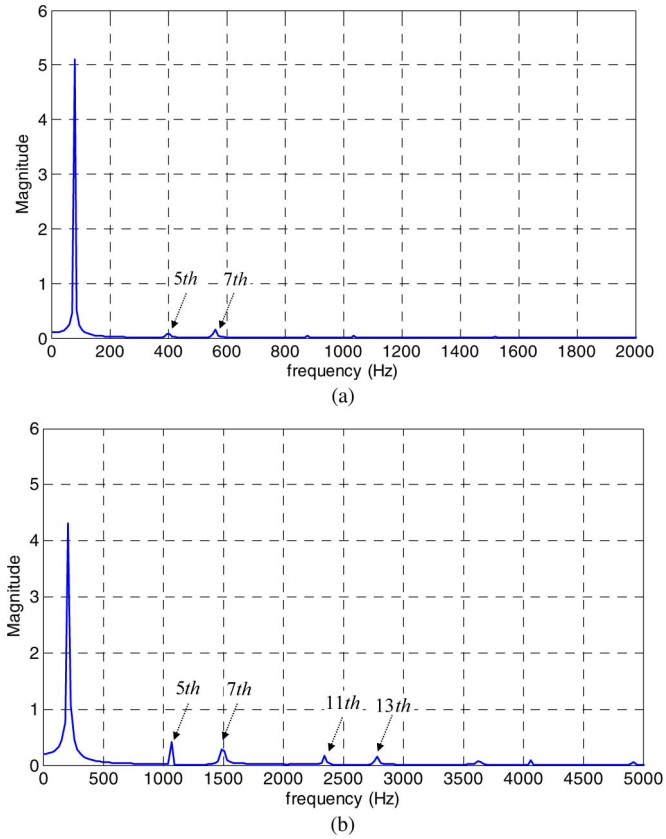

Fig. 7. FFT spectra of phase voltages. (a) FFT spectrum of phase voltage waveform of Fig. 6(a). (b) FFT spectrum of phase voltage waveform of Fig. 6(b).

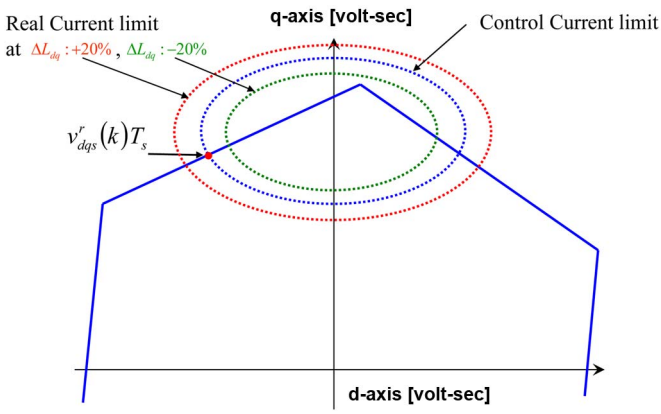

Fig. 8. Effect of parameter errors in the proposed WS-DTFC method.

while performing the WS-DTFC at the operational limit. When the voltage command is saturated due to large changes in torque command at low speeds, the modified voltage vector is naturally relocated on the voltage boundary by conventional overmodulation schemes because there is no intersection between voltage and current limit, as shown in Fig. 2. This implies that the proposed WS-DTFC strategy provides an inherent property to distinguish overmodulation from flux weakening operation without requiring extra parameters or control actions.

This structure leads to the single control law which avoids the complexity of having an additional control function or gain to be adjusted. This can never be achieved in existing CVC and DTFC schemes.

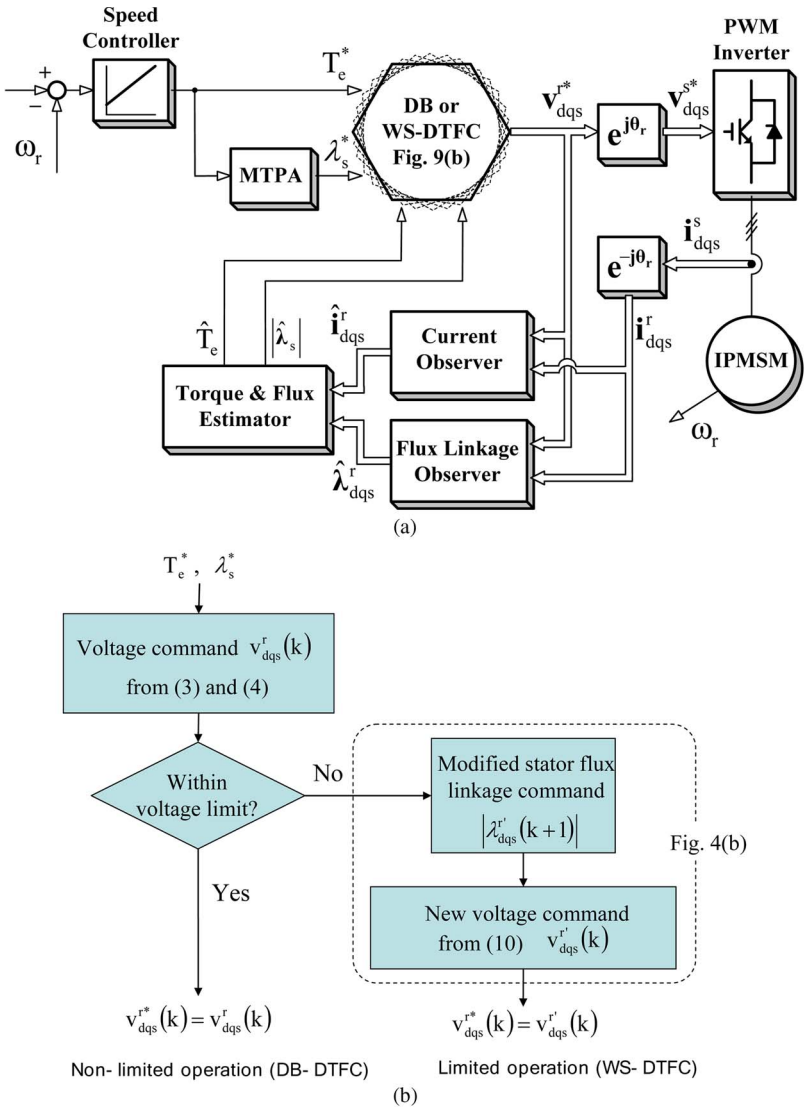

Fig. 9. Proposed DTFC strategy. (a) Overall, control structure. (b) Operational flow of the DB-DTFC or WS-DTFC.

IV. Experimental Results

The proposed WS-DTFC algorithm was implemented on a 900 W IPMSM, as described in Table I, coupled to a 1.0 kW ac servo motor. An encoder of 2500-pulse-per-revolution was mounted on one end of the test motor to measure the actual position. A fixed MTPA curve was implemented to utilize both the electromagnetic and reluctance torques available in the IPMSM below the base speed [9], [14]. The CVC and WS-DTFC were implemented in the inverter with a constant PWM sampling frequency of 10 kHz.

The test results of the conventional CVC method [12] are shown in Fig. 10, where the x–y plot of the stator voltage, air-gap torque, rotor speed, stator voltage magnitude, and the current magnitude are displayed from top to bottom. In this test, the dc link voltage was set to 150 V, and the IPMSM drive was operated with an infeasible speed command in order to saturate the speed controller. Here, the voltage feedback-based flux weakening control scheme was applied above the base speed. It can be observed from the x–y plot that the stator voltage moves along the voltage limit circle $(V_{\rm dc}/\sqrt{3})$ in the flux weakening region. Even though the controller fully uses the available voltage and current during wide-speed operation, the realization of maximum voltage utilization fails due to the linear voltage limit. The advent of flux weakening occurs at about 1200 r/min and the maximum speed is 2860 r/min.

TABLE I
Ratings and Nominal Parameters of 900 W IPMSM Under Test

Ratings and Parameters	Value	Unit
Rated torque	2.9	Nm
Number of poles	8	
R_s @25°C	1.82	Ω
L_q / L_d	20.2 / 8.5	mH
λ_{pm}	0.115	Wb

The same experiment was repeated using the proposed DTFC in the testing system, as shown in Fig. 11. The x–y stator

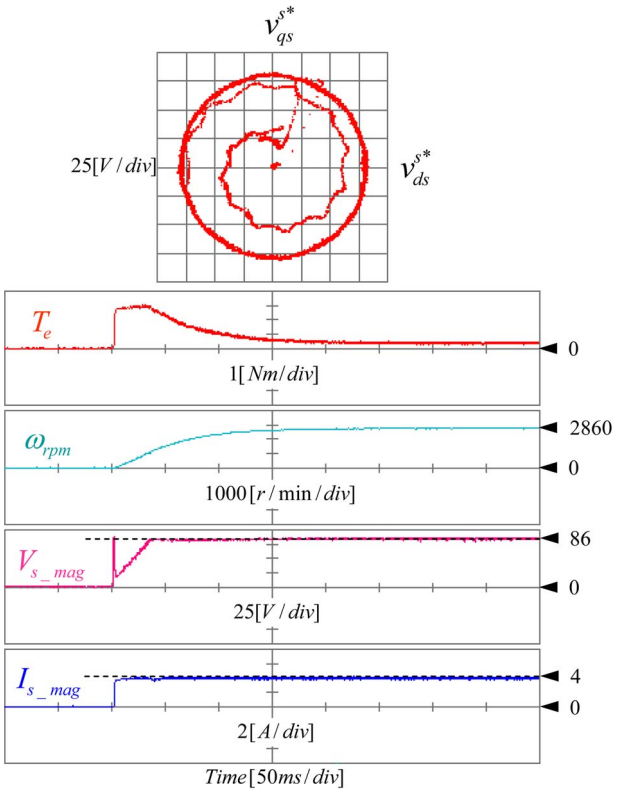

Fig. 10. Conventional CVC test results with linear voltage limit.

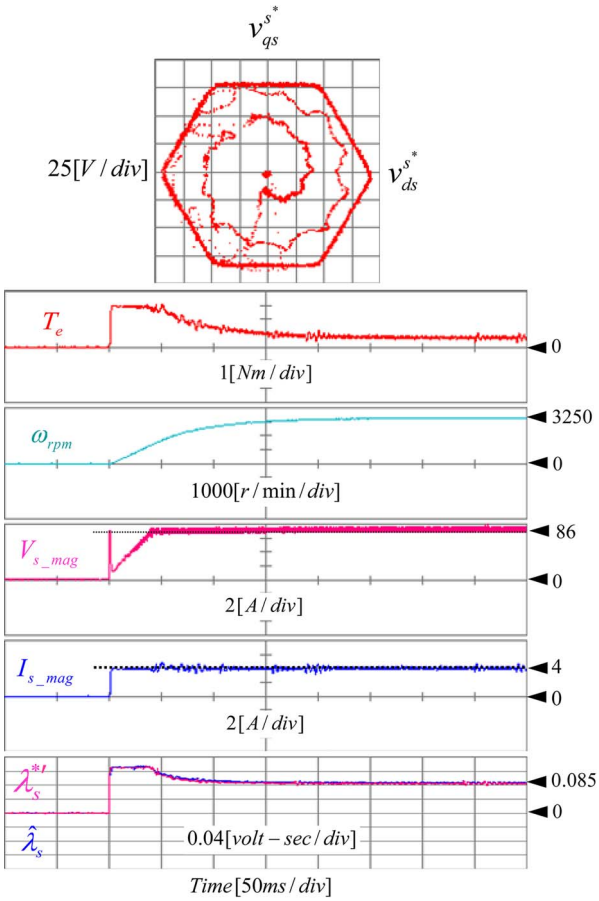

Fig. 11. Proposed wide-speed DTFC test results.

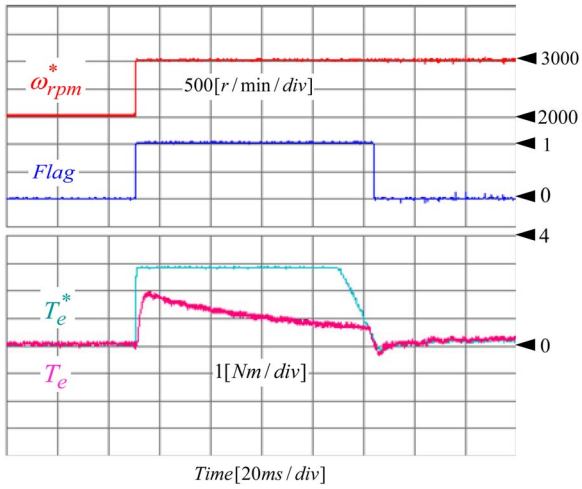

Fig. 12. Step torque response in the flux weakening region.

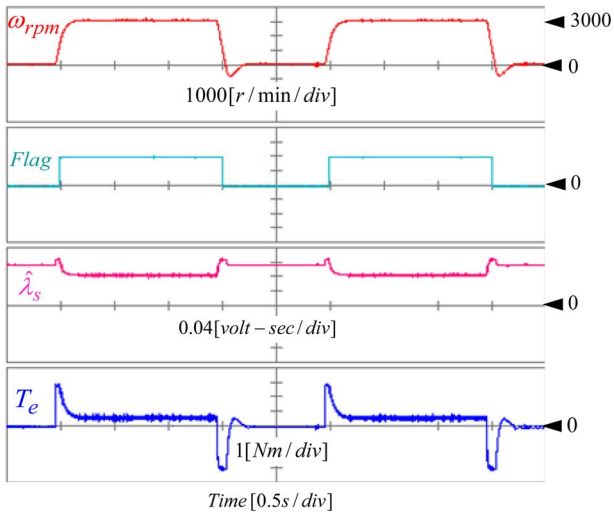

Fig. 13. Transient response with the speed command from zero to 3000 r/min.

voltage locus almost reaches its maximum voltage under limited conditions. In this test, the drive enters the flux weakening region at around 1300 r/min. The maximum speed is 3250 r/min, which represents an increase of 13.6% compared to the CVC result. The bottom plot shows the overlay waveforms of the modified stator flux linkage by (8) and the estimated stator flux linkage. It can be seen from the waveform of the air-gap torque and the stator flux that a smooth transition occurs between the non-limited operation and the flux weakening mode. The result indicates that the developed voltage selection approach was successfully applied to IPMSMs at the current and voltage limits. The resulting controller was proven to work without requiring any extra control gains, flux weakening control methods, and sophisticated anti-windup techniques over the entire operating space. The experimental results clearly show that maximum voltage utilization and improved torque production are achieved with a single control law.

The waveforms in Fig. 12 shows a step torque response of the proposed WS-DTFC in the flux weakening region, while the speed command was stepwise increased from 2000 r/min to 3000 r/min. From top to bottom, the speed command, the flag signal, the torque command, and the air-gap torque are

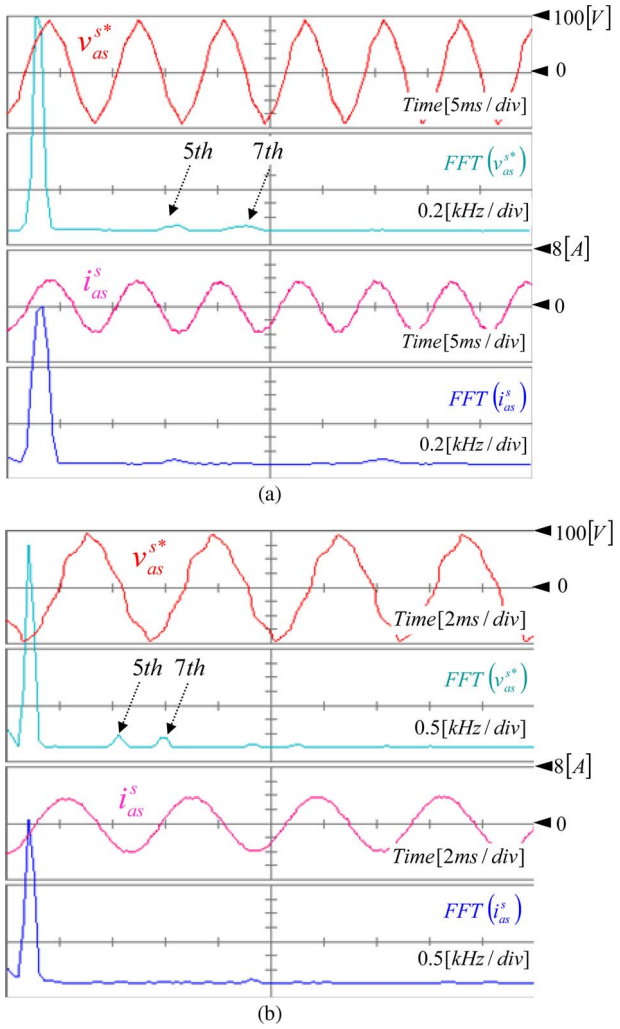

Fig. 14. Comparison of output voltage and current around the base and maximum speed. (a) Test results at the base speed. (b) Test results at the maximum speed.

depicted. The flag signal indicates that the command voltage vector lies outside of the voltage hexagon when the "Flag" equals to 1. In this transient region, the air-gap torque cannot follow the torque command due to the lack of the available inverter voltage. Thus, it takes finite settling steps to achieve a desired air-gap torque that is physically infeasible in one step. The intersection of the current limit and the rotating hexagon becomes the modified command voltage vector to achieve the fastest torque dynamics under the transient state.

The speed deceleration performance was investigated through experiments between zero and 3000 r/min, as shown in Fig. 13. From top to bottom, the controlled rotor speed, the flag signal, the estimated stator flux linkage, and the air-gap torque are depicted. Here, the flag signal indicates that the flux weakening control is performed when the "Flag" has the high state. Even during braking transients, the proposed WS-DTFC drive maintains the stable and reliable operation.

Another experimentation was carried out to assess the effects of add-on harmonics under different speeds. Fig. 14 shows the spectral comparison of the A-phase voltage and current waveform around the base and maximum speed. The unbalanced voltage selection interval results in more harmonics in the phase voltage at the maximum speed, but the add-on magnitude is relatively small compared to that of the fundamental component. The harmonics magnitudes in the current waveform make no difference because high-order harmonics are almost filtered out. This behavior may not be severe, or not be even problematic, for applications requiring the maximum voltage excitation.

V. Conclusion

In this paper, we investigated a wide-speed DTFC method associated with the physical constraints of IPMSMs. In the proposed approach, the drive system can provide fast and non-oscillatory dynamics under physical limits, since integrators are not employed for torque control or flux weakening. To support this conclusion, we provided a graphical and analytical analysis that naturally leads to a unique stator voltage trajectory for WS-DTFCs. This allows for the choice of an objective voltage vector extending the operational ranges. Motivated by these considerations, the transparent and streamlined controller can operate under a single control law and reduces the time and effort required for the calibration of the controller in the entire operating region.

References

[1] S. R. Macminn and T. M. Jahns, "Control techniques for improved high-speed performance of interior PM synchronous motor drives," *IEEE Trans. Ind. Appl.*, vol. 27, no. 5, pp. 997–1004, Sep./Oct. 1991.

[2] S. Morimoto, M. Sanada, and Y. Takeda, "Wide-speed operation of interior permanent magnet synchronous motors with high-performance current regulator," *IEEE Trans. Ind. Appl.*, vol. 30, no. 4, pp. 920–926, Jul./Aug. 1994.

[3] T. M. Jahns, "Flux-weakening regime operation of an interior permanent-magnet synchronous motor drive," *IEEE Trans. Ind. Appl.*, vol. IA-23, no. 4, pp. 681–689, Jul. 1987.

[4] A. Yoo and S. K. Sul, "Design of flux observer robust to interior permanent-magnet synchronous motor flux variation," *IEEE Trans. Ind. Appl.*, vol. 45, no. 5, pp. 1670–1677, Sep./Oct. 2009.

[5] T. S. Kwon, G. Y. Choi, M. S. Kwak, and S. K. Sul, "Novel flux-weakening control of an IPMSM for quasi-six-step operation," *IEEE Trans. Ind. Appl.*, vol. 44, no. 6, pp. 1722–1731, Nov./Dec. 2008.

[6] D. Casadei, G. Serra, A. Stefani, A. Tani, and L. Zarri, "DTC drives for wide speed range applications using a robust flux-weakening algorithm," *IEEE Trans. Ind. Electron.*, vol. 54, no. 5, pp. 2451–2461, Oct. 2007.

[7] Z. Xu and M. F. Rahman, "Direct torque and flux regulation of an IPM synchronous motor drive using variable structure control approach," *IEEE Trans. Power Electron.*, vol. 22, no. 6, pp. 2487–2498, Nov. 2007.

[8] I. Boldea, M. C. Paicu, G. D. Andreescu, and F. Blaabjerg, "Active flux DTFC-SVM sensorless control of IPMSM," *IEEE Trans. Energy Convers.*, vol. 24, no. 2, pp. 314–322, Jun. 2009.

[9] G. Foo and M. F. Rahman, "Sensorless direct torque and flux-controlled IPM synchronous motor drive at very low speed without signal injection," *IEEE Trans. Trans. Ind. Electron.*, vol. 57, no. 1, pp. 395–403, Jan. 2010.

[10] B. H. Kenny and R. D. Lorenz, "Stator-and rotor-flux based deadbeat direct torque control of induction machine," *IEEE Trans. Ind. Appl.*, vol. 39, no. 4, pp. 1093–1101, Jul./Aug. 2003.

[11] R. D. Lorenz, "The emerging role of dead-beat, direct torque and flux control in the future of induction machine drives," in *Proc. OPTIM Elect. Electron. Equipment Conf.*, May 2008, pp. 19–27.

[12] J. S. Lee, C. H. Choi, J. K. Seok, and R. D. Lorenz, "Deadbeat-direct torque and flux control of interior permanent magnet synchronous machines with discrete time stator current and stator flux linkage observer," *IEEE Trans. Ind. Appl.*, vol. 47, no. 4, pp. 1749–1758, Jul./Aug. 2011.

[13] S. H. Kim, C. H. Choi, and J. K. Seok, "Voltage disturbance state-filter design for precise torque-controlled interior permanent magnet synchronous motors," in *Proc. IEEE ECCE*, 2011, pp. 2445–2451.

[14] Y. Inoue, S. Morimoto, and M. Sanada, "A novel method of maximum-power operation for IPMSMs in DTC system," in *Proc. EPE*, 2009, pp. 1–10.

Chan-Hee Choi (S'06) received the B.S., M.S., and Ph.D. degrees from the School of Electrical Engineering, Yeungnam University, Kyungsan, Korea, in 2004, 2007, and 2012, respectively.

Currently, he is with the AE Control R&D Laboratory, LG Electronics Inc., Changwon, Korea. His specific research interests are high-performance electrical machine drives and sensorless drives of ac machine.

Jul-Ki Seok (S'94–M'98–SM'09) received the B.S., M.S., and Ph.D. degrees from Seoul National University, Seoul, Korea, in 1992, 1994, and 1998, respectively, all in electrical engineering.

From 1998 to 2001, he was a Senior Engineer with the Production Engineering Center, Samsung Electronics, Suwon, Korea. Since 2001, he has been a member of the Faculty of the School of Electrical Engineering, Yeungnam University, Kyungsan, Korea, where he is currently a Professor. His specific research areas are motor drives, power converter control of offshore wind farms, and nonlinear system identification related to the power electronics field.

Dr. Seok serves as the Chair of the IEEE Industry Applications Society (IAS) Industrial Drives Committee Paper Award Subcommittee, an Associate Editor of the IEEE TRANSACTIONS ON INDUSTRY APPLICATIONS, and the Editorial Board of the IET *Electric Power Applications*.

Robert D. Lorenz (S'83–M'84–SM'91–F'98) received the B.S., M.S., and Ph.D. degrees from the University of Wisconsin, Madison, and the M.B.A. degree from the University of Rochester, Rochester, NY.

Since 1984, he has been a member of the faculty of the University of Wisconsin, where he is the Mead Witter Foundation Consolidated Papers Professor of Controls Engineering in the Department of Mechanical Engineering. He is the Codirector of the Wisconsin Electric Machines and Power Electronics Consortium. It is the largest industrial research consortium on motor drives and power electronics in the world. Prior to joining the university, he worked 12 years in industry, in Rochester, principally on high-performance drives and synchronized motion control. He has authored over 260 published technical papers. He is the holder of 24 patents, with five more pending.

Dr. Lorenz was the IEEE Division II Director for 2005/2006, the IEEE Industry Applications Society (IAS) President for 2001, and a Distinguished Lecturer of the IEEE IAS for 2000/2001. He received the 2003 IEEE IAS Outstanding Achievement Award, 2006 EPE PEMC Outstanding Achievement Award, and 2011 IEEE IAS Distinguished Service Award. He has won 26 IEEE prize paper awards on power electronics, drives, self-sensing, current regulators, etc.